Advances in Materials Physics and Chemistry, 2014, 4, 43-49
Published Online March 2014 in SciRes. http://www.scirp.org/journal/ampc
http://dx.doi.org/10.4236/ampc.2014.43007

Mechano-Synthesized Orthoferrite Starting from Wüstite Assisted by SPS

Claudia Alicia Cortés-Escobedo[1*], Félix Sánchez-De Jesus[2], Ana María Bolarín-Miró[2], Sophie Nowak[3], Elizabeth Piazzini Juárez-Camacho[1], Sebastián Díaz de la Torre[1], Raúl Valenzuela[4]

[1]Instituto Politécnico Nacional, Centro de Investigación e Innovación Tecnológica, CIITEC, México D.F., México
[2]Universidad Autónoma del Estado de Hidalgo-AACTyM, Mineral de la Reforma, Pachuca, México
[3]ITODYS, UMR, CNRS 7086, Université de Paris-Diderot, Paris, France
[4]Instituto de Investigaciones en Materiales-UNAM, México D.F., México
Email: [*]claudia.alicia.cortes@gmail.com

Received 28 January 2014; revised 4 March 2014; accepted 11 March 2014

Abstract

Stoichiometric mixtures of FeO and Y_2O_3 were milled and heat treated to obtain yttrium iron garnet, $Y_3Fe_5O_{12}$. Two types of heating systems were used: one, a spark plasma sintering machine and the second, an electrical oven. The magnetic properties of the resulting specimens have been analyzed and discussed as a function of the grain size and the particles' morphology. The partial formation of garnet and orthoferrite phases was revealed on the obtained powder through microstructural analyses after 9 h of ball milling. The milled powders were transformed into the orthoferrite phase after the SPS-treatment at 700˚C and 900˚C. Magnetic-saturation studies revealed magnetic responses up to 12.7 emu/g for specimens SPS-treated at 700˚C, whereas 2.1 emu/g for samples SPS-treated at 900˚C. Conventionally treated specimens at 700˚C developed 0.36 emu/g of magnetization, while 0.93 emu/g was registered for those treated at 900˚C.

Keywords

Wüstite; Orthoferrite; Mechano-Synthesis; SPS; Magnetic Properties

1. Introduction

Yttrium iron garnet (YIG, $Y_3Fe_5O_{12}$) is a ferromagnetic material that has a wide range of applications in the communication field because it possesses the highest quality factor in the range 1 - 10 GHz, the bandwidth of

[*]Corresponding author.

microwave [1]-[3]. YIG is often used in devices such as circulators, isolators, oscillators, phase shifters for the microwave region like storage units, sensors, lasers, phosphorescent sources, and electrochemical devices. Its frequent use is due to its electromagnetic properties such as large Faraday rotation, low propagation loss, high and controllable saturation magnetization, moderate thermal expansion coefficients, energy transfer efficiency, and narrow line-width in ferromagnetic resonance [4] [5]. On the other hand, yttrium orthoferrite ($YFeO_3$) has been used as a magnetic insulator, for information processing, magneto-optical devices, cathodes and catalysts supports. This is due to its magnetic moment in the Fe sublattice, which is antiparallel, and its transparency in the visible and near infrared regions [6]-[10].

The conventional methods of obtaining YIG consist in a solid-state reaction of Fe_2O_3 and Y_2O_3 at high sintering temperatures (>1350˚C) and long sintering times (>10 h) in conventional furnaces [1] [4], leading to an increased particle size. Other techniques to obtain YIG are co-precipitation [5] [11] [12], auto-combustion of nitrate-citrate gel [13]-[15], spray plasma processes [15], and microwave [16] [17]. The conventional method of obtaining orthoferrite is mixing the precursor powders of Y_2O_3 and Fe_2O_3 in stoichiometric relation and heating to 1100˚C [1].

It is well known that magnetic properties such as the coercive field and saturation magnetization are strongly dependent upon the microstructure, shape, and size of crystals, crystal size distribution, and phase purity [4] [14].

The mechano-synthesis process is often carried out through an efficient high-energy ball milling technique that reduces processing time and energy consumption due to low operation temperatures. This converts mechanical energy into chemical energy [18]. However, since the spark plasma sintering (SPS) technique can be carried out within just few minutes, it allows for a lower temperature and shorter sintering time [19], while keeping the final products small grain sized.

Another important consideration has to be made regarding the magnetic properties related to non-stoichiometry. Many efforts have been made to produce mostly pure YIG, but only a few studies have been found to correlate nonstoichiometry and oxidation number effects on the final magnetic properties in both YIG and orthoferrite ceramics [20]-[22].

Fernández-García *et al* obtained bulk YIG specimens by calcining powder from 1000˚C to 1200˚C and starting from a mixture of Fe_2O_3 and Y_2O_3. Powders calcined at 1200˚C with further spark plasma sintering allowed for the appearance of orthoferrite peaks in the case of holding times at about 15 and 30 minutes [19].

This paper presents the effect of both processing and precursors in the final magnetic properties of $YFeO_3$ and $Y_3Fe_5O_{12}$ comparing solid-state reaction, mechano-synthesis plus SPS, and mechano-synthesis plus conventional heating in air and argon.

2. Experimental

Samples were prepared following four experimental routes, namely: 1) solid state reaction (SSR), 2) mechano-synthesis followed by conventional heat treatment (MSHT), 3) mechano-synthesis followed by spark plasma sintering (MSSPS), and 4) mechano-synthesis followed by heat treatment in argon (MSHTAr). In all cases, the precursor materials were the same: FeO and Y_2O_3 (Sigma Aldrich, 99.90% purity).

For the first processing route, SSR 1), stoichiometric amounts of FeO and Y_2O_3 powders were mixed for 15 min and then annealed at 700˚C or 900˚C for 3h in air to obtain YIG, following the reaction:

$$3/2Y_2O_3 + 5FeO_{(exc)} + O_{2\,(\text{from vial})} \rightarrow Y_3Fe_5O_{12-\delta} \quad (1)$$

For the MSHT route 2), stoichiometric amounts of FeO and Y_2O_3 powders as precursors, according to equation (1), were milled in air using a high-energy ball mill (SPEX 8000D) at room temperature for 9 h. Steel balls of 1.27 cm in diameter and a steel cylindrical vial of 50 cm^3 were used, setting up a ball to powder weight ratio of 10:1. This action was then applied alternatively with a 90 min cycle of milling, followed by a 30 min break. Powders were eventually annealed at 700˚C or 900˚C for 3 h in air.

In the case of the MSSPS route 3), the mixture of powders released after mechano-synthesis (90 min of milling) was sintered at 700˚C and 900˚C, with a heating rate of 100˚C/min, using the spark plasma sintering (SPS) apparatus Dr. Sinter 1050, applying 5KN of axial load and 6×10^{-2} Pa vacuum. The powder to be sintered was placed inside a graphite cylinder matrix of 10 mm diameter, setting holding times at 700˚C and/or 900˚C for 10 min.

Finally, MSHTAr route 4) was performed by heating mechano-synthesized powders in a chamber under Ar

atmosphere as part of an X-ray diffraction using Panalytical X-Pert Pro equipment from 25˚C to 950˚C.

Specimens obtained by the four different routes: SSR, MS, MSHT, and MSSPS, were characterized by X-ray diffractometry (XRD) using a Siemens D5000 diffractometer using CoKα_1 (λ = 1.7889 Å) radiation, while the MSHTAr sample was characterized in a Panalytical X-Pert Pro equipped with a multichannel detector (X'celerator) and by using Co-Kα radiation. The specimens' fracture morphology was analyzed using a field emission image FEI Quanta 3D FEG scanning electron microscope operated at 25 kV. The magnetic susceptibility and magnetization studies were performed at room temperature using an LDJ 9600 vibrating sample magnetometer with a maximum field of 16 kOe.

3. Results and Discussion

3.1. Structural Characterization

The X-ray diffraction patterns (XRD) of samples were obtained by different methods: i) as ball-milled powder for 9 hours, ii) Y_2O_3 and FeO powder conventionally heat-treated at 700˚C (SSR), iii) both mechano-synthesized and SPS-treated powder (MSSPS) at 700˚C, iv) both mechano-synthesized and conventionally heat treated (MSHT) specimens at 700˚C, and v) mechano-synthesized and heat treated under argon atmosphere (MSHTAr). These XRD patterns are shown in **Figure 1(a)**.

In the XRD corresponding to Y_2O_3 and FeO powder mixture milled for 9 hours (see **Figure 1(i)**), the formation of yttrium ferrite with both perovskite and garnet structures ($YFeO_3$ ICSD # 43260, $Y_5Fe_3O_{12}$ ICSD # 2012, respectively), being predominant in the orthoferrite phase, can be seen. A reflection peak of elemental iron, Fe^0 (ICSD # 64998), is also observed (marked with an arrow in the figure) which can be associated with a reduction of FeO. The evidence of wüstite, FeO (ICSD # 76639), as traces in this pattern is due to the excess of reactant originally introduced into the vial (regarding stoichiometric orthoferrite) in order to assure garnet structure. Meanwhile, isolated Y_2O_3 (ICSD # 78581) diffraction peaks were not detected in the as-milled condition. In the same **Figure 1(a)**, the X-ray diffraction patterns derived from the powder mixture subjected to the solid state reaction (SSR) route, heat treated at 700˚C, discloses mainly Fe_2O_3 and Y_2O_3 peaks, which suggest the partial oxidation of Fe^{2+} to Fe^{3+} due to the heating, whereas the garnet phase is neither detected nor are or thoferrite peaks observed. In the case of the sample MSSPS treated at 700˚C, the perovskite phase formation takes place, while the garnet phase almost disappears. In this pattern, the FeO peaks were not detected, but the presence of Fe^0 peaks is evident. Although in the XRD patterns corresponding to the MSHT route, the most important phase

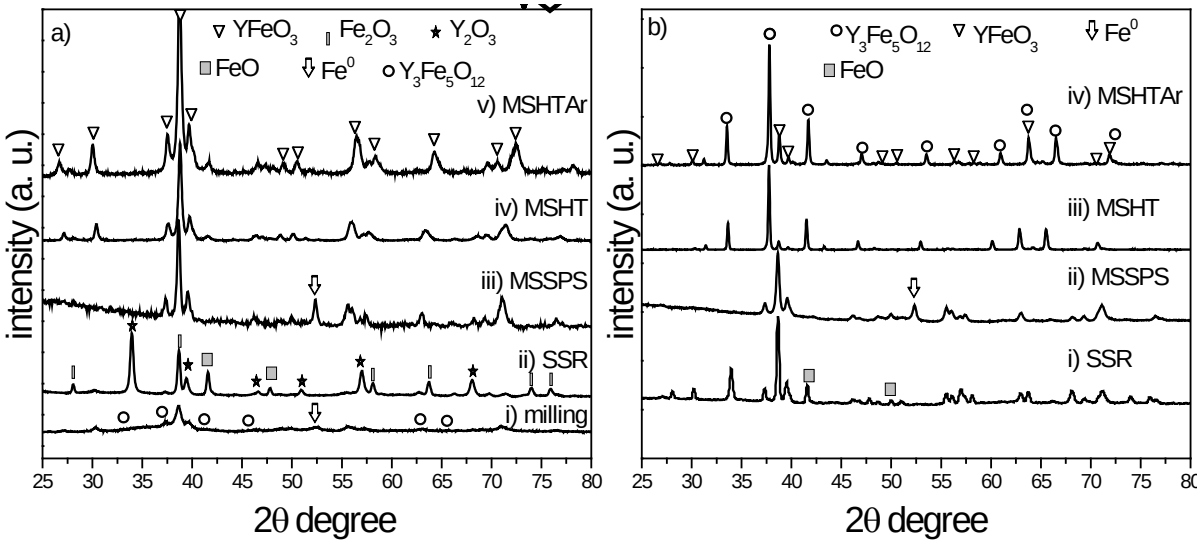

Figure 1. X-ray powder diffraction patterns of: i) FeO + Y_2O_3 as milled; ii) SSR: mixture heat treated at 700˚C; iii) MSSPS: samples milled and spark plasma sintered at 700˚C; iv) MSHT: samples milled and heat treated at 700˚C; v) MSHTAr: mechano-synthesized powders heat treated under argon atmosphere at 700˚C; vi) SSR: mixture heat treated at 900˚C; vii) MSSPS: samples milled and spark plasma sintered at 900˚C; viii) MSHT: samples milled and heat treated at 900˚C and ix) MSHTAr: mechano-synthesized powders heat treated under argon atmosphere at 900˚C.

detected is perovskite. The Fe_2O_3 (ICSD # 43465) phase was found, which indicates an oxidation of FeO, as in SSR route. Also, it is observed for a sample heat treated under argon atmosphere, MSHTAr, that the presence of Fe_2O_3 is as that heat treated in air, but there is also a small peak for Fe^0.

For all analyzed cases in **Figure 1(a)** diffraction peaks become narrow and sharp where their intensities increase which implies the grain growth in the microstructure of products, as long as the powder is heated.

The X-ray diffraction patterns of the next samples: vi) conventionally heat-treated FeO and yttria powder mixture at 900˚C (SSR), vii) as ball-milled powder for 9 hours and SPS sintered (MSSPS) specimens at 900˚C, and viii) mechano-synthesized and annealed specimens (MSHT), and ix) mechano-synthesized powders heat treated under argon atmosphere at 900˚C are shown in **Figure 1(b)**. In the case of the solid-state reaction (SSR), the diffraction XRD pattern predominantly shows the presence of the orthoferrite phase, and also hematite and yttrium oxide peaks. In this pattern, diffraction peaks of the garnet phase were not detected. As for the powder mixture treated by MSSPS at 900˚C, the XRD pattern showed a complete disappearance of YIG. Here, the Y_2O_3 and FeO peaks were detected. Despite that diffraction, peaks of Fe_2O_3 were observed to disappear at 700˚C and 900˚C, but the elemental Fe^0 peak remains. Both perosvkite and garnet phases were detected for the MSHT-sample, the latter acting as the major phase.

By contrast to **Figure 1(a)**, the Bragg peaks reported in **Figure 1(b)** obtained after any treatment at 900˚C do present narrower and enlarged peaks (large relative intensities) indicating a growth of grains.

The Rietveld refinement results for the weight percentage of each phase obtained from the XRD patterns analyses are presented in **Table 1**. These results confirm the microstructural behavior previously described.

3.2. Scanning Electron Microscopy

The scanning electron microscopy (SEM) images of samples sintered at 700˚C with SPS (MSSPS) are presented in **Figure 2**. **Figure 2(a)**, annealed (MSHT) and **Figure 2(b)**, solid-state reaction (SSR). **Figure 2(c)** shows that particles are highly agglomerated and the grain size is not uniform; the grains do not have a regular shape.

Morphology of the fracture for samples sintered at 900˚C with SPS is shown in **Figure 3(a)**. Here, it is observed that the formation of particles with acute edges is associated with the orthoferrite phase. On the other hand, the mechano-synthesis plus annealed sample of **Figure 3(b)** clearly shows neck formation. In both series of samples (**Figures 2** and **3**) grain growth can be seen. In the sample of solid-state reaction **Figure 3(c)** the formation of liquid-like morphology for joint, but not compacted, particles can be observed.

3.3. Magnetic Properties

The magnetic hysteresis loops recorded from specimens processed and sintered by the experimental routes explained in this work are shown in **Figure 4**. On the left side of **Figure 4**, samples treated at 700˚C are shown, whereas their counterparts treated at 900˚C are shown to the right. There are clear differences in the magnetic response of specimens obtained from the proposed routes. The largest saturation of magnetization induced into the powder mixture, as studied in this work, is attained when following the mechano-synthesis route with subsequent annealing (MSHT) at 900˚C; *i.e.*, specimens could develop values in the order of 25 emu/g, which is close to that of bulk (26 emu/g) [15], even with the presence of $YFeO_3$, which should reduce its magnetization due to its canted antiferromagnetic behavior [29]. This is followed by the mechano-synthesized specimens with subsequent SPS treatment at 700˚C leading to values around 12.7 emu/g, this magnetic behavior can be influ-

Table 1. Data from Rietveld refinement of XRD patterns in each method.

Weight %	Milled 9 h	MSSPS 700˚C	MSHT 700˚C	SSR 700˚C	MSSPS 900˚C	MSHT 900˚C	SSR 900˚C
FeO [23]	1.7	0	0	0	2.53	0	0
Y_2O_3 [24]	0.6	0	0.18	44.87	0.67	0	21.86
$Y_3Fe_5O_{12}$ [25]	44.6	3.55	0.36	0	0	89.73	2.12
$YFeO_3$ [26]	49.9	81.19	84.47	8.12	90.85	10.27	46.08
Fe^0 [27]	3.2	15.26	0	0	5.95	0	0
Fe_2O_3 [28]	0	0	14.94	47.01	0	0	29.94

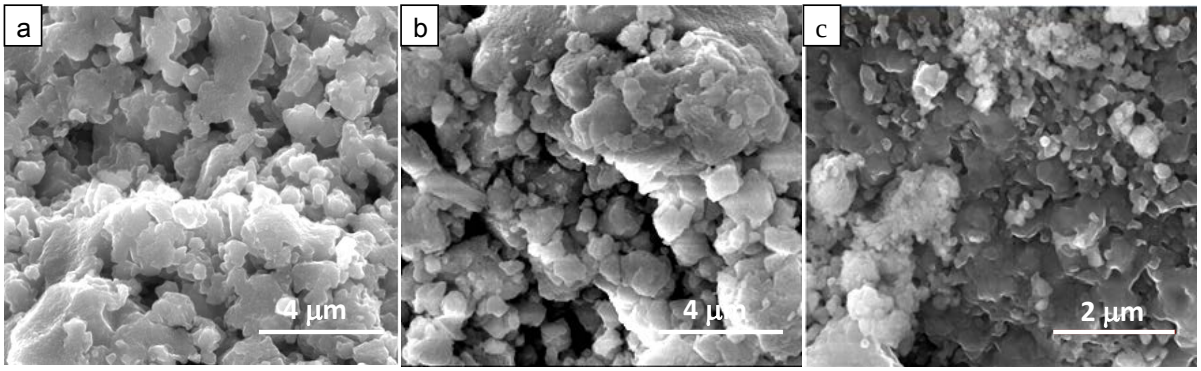

Figure 2. SEM images of the powder mixture after (a) mechano-synthesis plus SPS at 700˚C; (b) mechano-synthesis plus heat treatment at 700˚C and (c) solid state reaction at 700˚C.

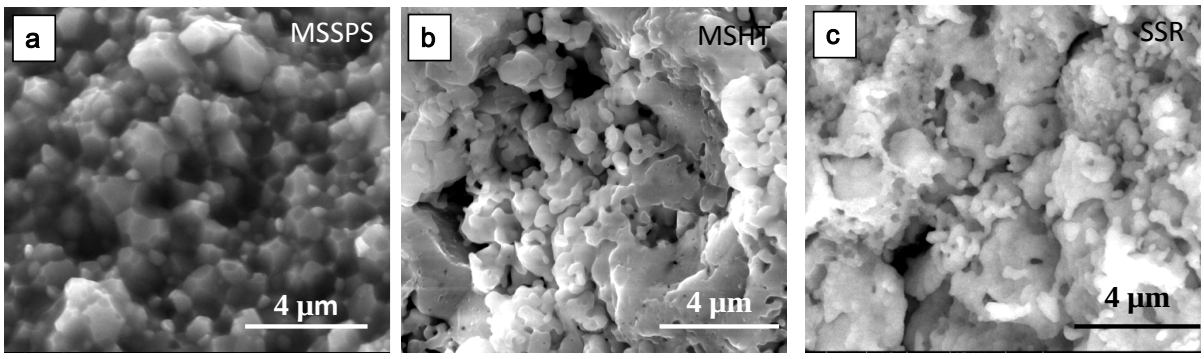

Figure 3. SEM images of the powder mixture after (a) mechano-synthesis plus SPS at 900˚C; (b) mechano-synthesis plus annealing treatment at 900˚C and (c) solid state reaction at 900˚C.

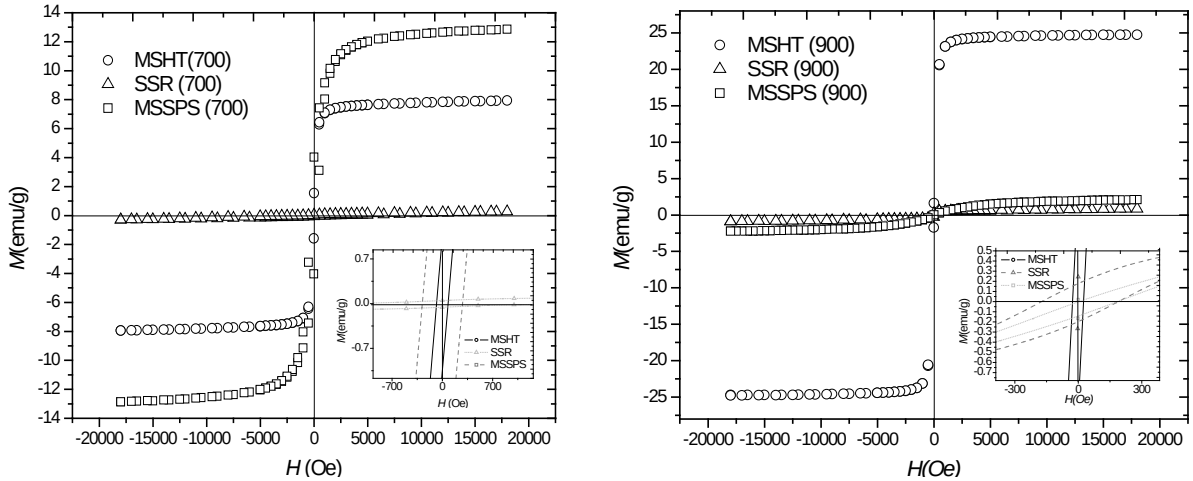

Figure 4. Saturation magnetization (Ms) measured at room temperature for YIG obtain of different methods at 700˚C and 900˚C.

enced by the presence of Fe^0, increasing the saturation magnetization due to its high values (~221 emu/g) [30]. In the processing case of solid-state reaction, the saturation magnetization of samples treated at 700˚C and 900˚C are 0.36 and 0.96 emu/g, respectively. Contrary to what was expected, mixtures obtained do not follow an ideal behavior, *i.e.* there are interactions between them, which increases its saturation magnetization. On the other hand, as expected, the coercive field seems to be higher for MSSPS samples (see **Figure 4**) due to lower particle size, only in the case of 700˚C treatment. In the case of 900˚C, MSSPS samples show a diminution in its

coercivity associated with grain growth, as is shown in **Figure 3(a)**.

4. Conclusion

Four experimental routes have been analyzed in this work as to the preparation of YIG materials, starting from wüstite, FeO, and ittria Y_2O_3 powders. When such a ceramic powder mixture is heat-treated, it undergoes different phase precipitations, but without garnet formation, after 900˚C, mainly orthoferrite is obtained. The mechano-synthesis processing route followed by heat treatment (MSHT), as conducted in this work, has been shown to be the most convenient method to increase the $Y_3Fe_5O_{12}/YFeO_3$ ratio, thus improving the magnetic properties. On the other hand, the precipitation of $YFeO_3$ crystals with larger grain sizes occurring after the SPS treatment at 900˚C provides clear indications on the garnets' decomposition, due to the severe sintering conditions causing an increment in coercive field and diminution in magnetization saturation. Finally, reducing atmosphere for SPS samples as for heat-treated samples under argon allows the reduction of iron oxide to metallic iron.

Acknowledgements

Authors would like to thank Centro de Nanociencias, Micro y Nanotecnología del Instituto Politécnico Nacional, in particular to Dr. José Alberto Andraca Adame, Dr. Hugo Martínez Gutiérrez and MSc. Ricardo Escalona for structural, morphological characterization, and SPS sintering, respectively. Thanks are also due to SIP-IPN and CONACYT for financial support under grants SIP MULTI-1540, CB-157925, and CB-130413.

References

[1] Ali, W.F.F.W., Othman, M., Ain, M.F. and Abdullah, N.S. (2013) Studies on the Formation of Yttrium Iron Garnet (YIG) through Stoichiometry Modification Prepared by Conventional Solid-State Method. *Journal of the European Ceramic Society*, **33**, 1317-1324. http://dx.doi.org/10.1016/j.jeurceramsoc.2012.12.016

[2] Paesano Jr., A., Zanatta, S.C., de Medeiros, S.N., Cótica, L.F. and da Cunha, J.B. (2005) Mechanosynthesis of YIG and GdIG: A Structural and Mössbauer Study. *Hyperfine Interactions*, **161**, 211-220. http://dx.doi.org/10.1007/s10751-005-9193-1

[3] Mergen, A. and Qureshi, A. (2008) Characterization of YIG Nanopowders by Mechanochemical Synthesis. *Journal of Alloys and Compounds*, **478**, 741-744. http://dx.doi.org/10.1016/j.jallcom.2008.11.133

[4] Garskaite, E., Gibson, K., Leleckaite, A., Glaser, J., Niznansky, D., Kareiva, A. and Meyer, H.J. (2006) On the Synthesis and Characterization of Iron-Containing Garnets ($Y_3Fe_5O_{12}$, YIG and $Fe_3Al_5O_{12}$, IAG). *Chemical Physics*, **323**, 204-210. http://dx.doi.org/10.1016/j.chemphys.2005.08.055

[5] Rashad, M.M., Hessien, M.M., El-Midany, A. and Ibrahim, I.A. (2008) Effect of Synthesis Conditions on the Preparation of YIG Powders via Co-Precipitation Method. *Journal of Magnetism and Magnetic Materials*, **321**, 3752-3757. http://dx.doi.org/10.1016/j.jmmm.2009.07.033

[6] Rossol, F.C. (1970) Domain-Wall Mobility in Yttrium Orthoferrite. *Physical Review Letters*, **24**, 1021-1023. http://dx.doi.org/10.1103/PhysRevLett.24.1021

[7] Didosyan, Y.S. and Hauser, H. (1998) Observation of Bloch Lines in Yttrium Orthoferrite. *Physics Letters A*, **238**, 395-397. http://dx.doi.org/10.1016/S0375-9601(97)00757-3

[8] Didosyan, Y.S. and Barash, V.Y. (1995) Faraday Effect in Yttrium Orthoferrite in the Range 1280 - 1600 nm. *Journal of Magnetism and Magnetic Materials*, **151**, 207-210. http://dx.doi.org/10.1016/0304-8853(95)00374-6

[9] Rajendran, M. and Bhattacharya, A.K. (2006) Nanocrystalline Orthoferrite Powders: Synthesis and Magnetic Properties. *Journal of the European Ceramic Society*, **26**, 3675-3679. http://dx.doi.org/10.1016/j.jeurceramsoc.2006.01.008

[10] Didosyan, Y.S., Hauser, H., Wolfmayr, H., Nicolics, J. and Fulmek, P. (2003) Magneto-Optical Rotational Speed Sensor. *Sensors and Actuators A*, **106**, 168-171. http://dx.doi.org/10.1016/S0924-4247(03)00158-4

[11] Fernández-García, L., Suarez, M. and Menéndez, J.L. (2010) Synthesis of Mono and Multidomain YIG Particles by Chemical Coprecipitation or Ceramic Procedure. *Journal of Alloys and Compounds*, **495**, 196-199. http://dx.doi.org/10.1016/j.jallcom.2010.01.119

[12] Zhang, W., Guo, C., Ji, R., Fang, C. and Zeng, Y. (2011) Low-Temperature Synthesis and Microstructure-Property Study of Single-Phase Yttrium Iron Garnet (YIG) Nanocrystals via a Rapid Chemical Coprecipitation. *Materials Chemistry and Physics*, **125**, 646-651. http://dx.doi.org/10.1016/j.matchemphys.2010.10.004

[13] Hosseini Vajargah, S., Madaah Hosseini, H.R. and Nemati, Z.A. (2007) Preparation and Characterization of Yttrium

Iron Garnet (YIG) Nanocrystalline Powders by Auto-Combustion of Nitrate-Citrate Gel. *Journal of Alloys and Compounds*, **430**, 339-343. http://dx.doi.org/10.1016/j.jallcom.2006.05.023

[14] Vaqueiro, P., López-Quintela, M.A., Rivas, J. and Greneche, J.M. (1997) Annealing Dependence of Magnetic Properties in Nanostructured Particles of Yttrium Iron Garnet Prepared by Citrate Gel Process. *Journal of Magnetism and Magnetic Materials*, **169**, 56-68. http://dx.doi.org/10.1016/S0304-8853(96)00728-7

[15] Guo, X.Z., Ravi, B.G., Devi, P.S., Hanson, J.C., Margolies, J., Gambino, R.J., Parise, J.B. and Sampath, S. (2005) Synthesis of Yttrium Iron Garnet (YIG) by Citrate-Nitrate Gel Combustion and Precursor Plasma Spray Processes. *Journal of Magnetism and Magnetic Materials*, **295**, 145-154. http://dx.doi.org/10.1016/j.jmmm.2005.01.007

[16] Yang, Q., Zhang, H., Liu, Y., Wen, Q. and Jia, L. (2008) The Magnetic and Dielectric Properties of Microwave Sintered Yttrium Iron Garnet (YIG). *Materials Letters*, **62**, 2647-2650. http://dx.doi.org/10.1016/j.matlet.2008.01.040

[17] Fu, Y., Lin, C., Tay, K. and Yao, Y. (2008) Yttrium Iron Garnet Ceramic Prepared from Microwave-Induced Combustion. *Journal of Electroceramics*, **21**, 677-680. http://dx.doi.org/10.1007/s10832-007-9270-8

[18] Suryanarayana, C. (2004) Mechanical Alloying and Milling. Marcel Dekker, New York. http://dx.doi.org/10.1201/9780203020647

[19] Fernández-García, L., Suárez, M. and Menéndez, J.L. (2010) Low Temperature Spark Plasma Sintering of YIG Powders. *Journal of Alloys and Compounds*, **502**, 132-135. http://dx.doi.org/10.1016/j.jallcom.2010.04.117

[20] Jacob, K.T. and Rajitha, G. (2012) Nonstoichiometry, Defects and Thermodynamic Properties of $YFeO_3$, YFe_2O_4 and $Y_3Fe_5O_{12}$. *Solid State Ionics*, **224**, 32-40. http://dx.doi.org/10.1016/j.ssi.2012.07.003

[21] Veres, A., Noudem, J. G., Fourrez, S. and Bailleul, G. (2006) The Influence of Iron Substitution to Manganese on the Physical Properties of $YMnO_3$. *Solid State Sciences*, **8**, 137-141. http://dx.doi.org/10.1016/j.solidstatesciences.2005.11.002

[22] Cortés-Escobedo, C.A., Bolarín-Miró, A.M., Sánchez de Jesús, F., Valenzuela, R., Juárez Camacho, E.P. and Ammar, S. (2013) $Y_3Fe_5O_{12}$ Prepared by Mechanosynthesis from Different Iron Sources. *Advances in Materials Physics and Chemistry*, **3**, 41-46. http://dx.doi.org/10.4236/ampc.2013.31A006

[23] Benard, J. (1949) Recherches sur les variations de composition du protoxyde de fer. *Bulletin de la Societé Chimique de France*, 109-116.

[24] Paton, M.G. and Maslen, E.N. (1965) A Refinement of the Crystal Structure of Yttria. *Acta Crystallographica B*, **19**, 307-310. http://dx.doi.org/10.1107/S0365110X65003365

[25] Bonnet, M., Delapalme, A., Fuess, H. and Thomas, M. (1975) Refinement of the Structure of Yttrium Iron Garnet (YIG). A Case of Severe Extinction and Absorption. *Acta Crystallographica Section B*, **31**, 2233-2240. http://dx.doi.org/10.1107/S0567740875007315

[26] Wu, A., Shen, H., Xu, J., Wang, Z., Jiang, L., Luo, L., Yuan, Sh., Cao, Sh. and Zang, H. (2012) Crystal Growth and Magnetic Property of $YFeO_3$ Crystal. *Bulletin of Materials Science*, **35**, 259-263. http://dx.doi.org/10.1007/s12034-012-0278-6

[27] Owen, E.A and Williams, G.I. (1948 A Low-Temperature X-Ray Camera. *Journal of Scientific Instruments*, **25**, 440-444.

[28] Blake, R.L., Hessevick, R.E., Zoltai, T. and Finger, L.W. (1966) Refinement of the Hematite Structure. *American Mineralogist*, **51**, 123-129.

[29] Gil, D.M., Navarro, M.C., Lagarrigue, M.C., Guimpel, J., Carbonio R.E. and Gómez, M.I. (2011) Synthesis and Structural Characterization of Perovskite $YFeO_3$ by Thermal Decoposition of a Cyanocomplexprecursory$[Fe(CN6)]\cdot 4H_2O$. *Journal of Thermal Analysis and Calorimetry*, **183**, 889-896. http://dx.doi.org/10.1007/s10973-010-1176-z

[30] Danan, H., Herr, A. and Meyer, A.J.P. (1968) New Determinations of the Saturation Magnetization of Nickel and Iron. *Journal of Applied Physics*, **39**, 669-670. http://dx.doi.org/10.1063/1.2163571